Abdominal Radiology (2021) 46:636–646
https://doi.org/10.1007/s00261-020-02695-0

PANCREAS

Optimal target *b*-value on computed diffusion-weighted magnetic resonance imaging for visualization of pancreatic ductal adenocarcinoma and focal autoimmune pancreatitis

Shintaro Ichikawa[1] · Marie-Luise Kromrey[1,2] · Utaroh Motosugi[1,3] · Hiroshi Onishi[1]

Received: 1 June 2020 / Revised: 21 July 2020 / Accepted: 25 July 2020 / Published online: 1 August 2020

Abstract

Purpose To compare computed diffusion-weighted imaging (cDWI) feasibility with that of directly acquired DWI for visualizing pancreatic ductal adenocarcinoma (PDAC) and focal autoimmune pancreatitis (AIP).

Methods From April 2012 to January 2017, 135 patients with PDAC ($n = 111$) or focal AIP ($n = 24$) were retrospectively enrolled. They underwent DWI with *b*-values of 0, 500, and 1000 s/mm^2. From DWI_0 and DWI_{1000}, we generated cDWIs with targeted *b*-values of 1500, 2000, and 3000 s/mm^2. The lesions' signal intensities, image quality, signal intensity ratio (SIR) of lesions and pancreatic parenchyma to spinal cord, and lesion-to-pancreatic parenchyma contrast ratio (CR) were compared among the five DWI protocols (DWI_{500}, DWI_{1000}, $cDWI_{1500}$, $cDWI_{2000}$, and $cDWI_{3000}$). SIR was analyzed by receiver operating characteristic (ROC) analyses.

Results DWI_{500}, DWI_{1000}, and $cDWI_{1500}$ had higher image quality than $cDWI_{2000}$ and $cDWI_{3000}$ ($P < 0.001$). The incidence of clear hyperintense PDAC was highest on $cDWI_{2000}$, followed by $cDWI_{1500}$, and $cDWI_{3000}$ ($P < 0.001$–0.002), while the incidence of clear hyperintense AIP was higher on DWI_{1000}, $cDWI_{1500}$, and $cDWI_{2000}$ than on DWI_{500} and $cDWI_{3000}$ ($P = 0.001$–0.022). SIRs decreased whereas CRs increased as the *b*-value increased, for both PDAC and AIP. The area under the ROC curve (AUC) of SIR_{lesion} was significantly lower on $cDWI_{1500}$ than on $cDWI_{2000}$ and $cDWI_{3000}$ ($P < 0.001$).

Conclusion $cDWI_{1500}$ or $cDWI_{2000}$ generated from *b*-values of 0 and 1000 s/mm^2 were the most effective for visualizing PDAC and focal AIP; however, the SIR_{lesion} AUC was significantly lower on $cDWI_{1500}$ than on $cDWI_{2000}$ and $cDWI_{3000}$.

Keywords Magnetic resonance imaging · Computed diffusion-weighted imaging · Pancreas · Adenocarcinoma · Autoimmune pancreatitis

Introduction

Pancreatic cancer is the seventh leading cause of global cancer deaths in industrialized countries [1] and the third leading cause of cancer-related deaths in the United States [2]. Pancreatic ductal adenocarcinoma (PDAC) is the most common type of pancreatic cancer, accounting for 90% of all pancreatic cancers [3]. Despite the advancement of diagnostic techniques, early diagnosis of PDAC is still challenging, and its incidence is estimated to continue to increase [4]. Autoimmune pancreatitis (AIP) is a rare autoimmune disorder that can cause similar symptoms to PDAC [5]. Diffuse enlargement of the pancreas (sausage-like) and low-attenuating rim-like capsule on contrast-enhanced computed tomography are well-known typical imaging findings of AIP [5]; however, 21.7–60.0% of AIP present as focal mass-forming pancreatitis [6–9]. Treatment options are completely different between AIP and PDAC; therefore, accurate differential diagnosis is required. Several reports have shown that magnetic resonance imaging (MRI) might be useful for distinguishing focal AIP from PDAC [6–12]; however, such differentiation remains challenging.

Diffusion-weighted imaging (DWI) has been used routinely in daily clinical practice owing to its excellent contrast

✉ Shintaro Ichikawa
sichikawa@yamanashi.ac.jp

[1] Department of Radiology, University of Yamanashi, 1110 Shimokato, Chuo-shi 409-3898, Yamanashi, Japan

[2] Department of Diagnostic Radiology and Neuroradiology, University Medicine Greifswald, Greifswald, Germany

[3] Department of Diagnostic Radiology, Kofu Kyoritsu Hospital, Kofu, Yamanashi, Japan

resolution between lesions and the pancreatic parenchyma, without the use of contrast agents. Its usefulness in the detection and characterization of pancreatic diseases has been reported [13–15]. DWI with *b*-values of 800–1000 s/mm^2 is widely used; however, higher *b*-values can be useful for the detection and characterization of PDAC [16] because diffusion-restricted tissues show relatively higher signal intensity (SI) than the normal pancreatic parenchyma with the increasing *b*-values. However, DWI with higher *b*-values has certain disadvantages, including the longer acquisition time and poorer image quality [16]. Computed DWI (cDWI) is a technique that can synthesize arbitrary target *b*-value DWI from a set of directly acquired *b*-value images by voxel-wise fitting [17]. cDWI can generate images with a higher diffusion effect than that achieved by clinical MRI units, as well as a higher signal-to-noise ratio in shorter acquisition time than with directly acquired DWI [17].

The usefulness of cDWI has been reported for several organs, such as the prostate [18], breast [19], liver [20], uterus [21], ovary [22], and middle ear [23]; however, only few reports are available on pancreatic cDWI [24, 25]. Moreover, several studies have reported the usefulness of DWI for AIP diagnosis [9–11], whereas the usefulness of cDWI in AIP has not been clarified. Thus, the purpose of this study was to assess the feasibility of cDWI in visualizing PDAC and focal AIP comparison with that of directly acquired DWI.

Materials and methods

Patients

This single-center, retrospective, cross-sectional study was approved by the relevant institutional review board, who waived the requirement for obtaining written informed patient consent due to the retrospective nature of the study. Patients with PDAC or AIP were consecutively enrolled between April 2012 and January 2017. The following inclusion criteria were used for PDAC: (i) pathologically diagnosed by fine needle aspiration or resection, and (ii) availability of 3.0-T MRI data within three months before fine needle aspiration or resection; for AIP, the criteria were (i) clinically diagnosed based on clinical diagnostic criteria in Japan (JPS2011) [26], (ii) availability of 3.0-T MRI data before steroid therapy, and iii) focal type.

Of the 181 patients enrolled for the study, 46 patients were excluded (Fig. 1). The final study cohort consisted of 135 patients (mean age, 68.2 ± 10.2 [range 40–88] years), including 111 patients with PDAC and 24 with AIP (Fig. 1).

DWI protocols

All MRI examinations were performed using a 3.0-T MR system (Discovery 750; GE Healthcare, Waukesha, WI, USA) with a 32-channel phased-array coil. The DWI data were acquired in the transverse plane by respiratory-triggered single-shot echo-planar imaging with water-selective excitation, using the respiratory triggering technique. Sections of 5 mm in thickness with no intersection gap were used to cover the pancreas. The following three *b*-values were used: 0, 500, and 1000 s/mm^2, with three axes [*x* (RL),

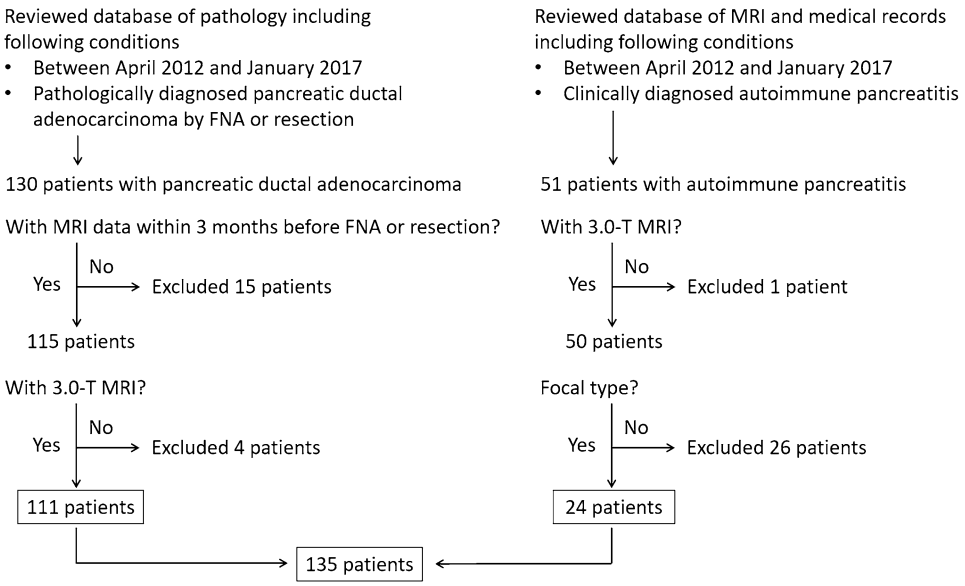

Fig. 1 Flowchart of patients' enrollment. Of the 181 patients enrolled for the study, 46 patients were excluded. The final study cohort consisted of 135 patients, including 111 patients with pancreatic ductal adenocarcinoma and 24 with autoimmune pancreatitis. *FNA* fine needle aspiration, *MRI* magnetic resonance imaging

y (AP), and *z* (SI)] motion-probing gradient directions. The pulse sequence parameters were as follows: repetition time, 3000–10000 ms (based on the respiratory interval); echo time, 70 ms; flip angle, 90°; field of view, 36 × 36 cm; matrix, 128 × 192; number of excitations, 8; sensitivity encoding acceleration factor, 2; and acquisition time, 150–180 s. Then, DW images with *b*-values of 0 and 1000 s/mm^2 were digitally transferred to dedicated post-processing software (SYNAPSE VINCENT; FUJIFILM Medical, Tokyo, Japan), and cDW images were generated with target *b*-values of 1500 ($cDWI_{1500}$), 2000 s/mm^2 ($cDWI_{2000}$), and 3000 s/mm^2 ($cDWI_{3000}$) by fitting a mono-exponential model, to compare them with the directly acquired DW images with *b*-values of 500 (DWI_{500}) and 1000 s/mm^2 (DWI_{1000}).

Qualitative image analysis

The directly acquired DW images (DWI_{500} and DWI_{1000}) and the cDW images ($cDWI_{1500}$, $cDWI_{2000}$, and $cDWI_{3000}$) were reviewed by two independent radiologists (with 11 and 3 years of clinical experience in abdominal MRI) who were blinded to the clinical data aside from the information that the patients had PDAC or AIP based on other MRI sequences. For each dataset, the two radiologists evaluated the image quality using a 4-point visual score (4, excellent = the whole pancreas is clearly shown without artifacts; 3, good = minor degradation is present but suitable for the evaluation of the whole pancreas; 2, fair = only part of the pancreas is visible; 1, poor = the pancreas is barely visible) (Fig. 2a) and classified the SIs of the lesions, as follows: type 1, clearly demarcated hyperintensity relative to the surrounding pancreas; type 2, hyperintensity, but with an unclear distal (tail sided) border because of hyperintense distal pancreatic parenchyma; and type 3, iso-intensity relative to the surrounding pancreas or no evidence of the lesions (invisible) [16, 24] (Fig. 2b).

Quantitative image analysis

The same radiologists who performed qualitative image analysis also conducted quantitative measurements for the following: (a) the signal intensity ratio (SIR) of the lesions and proximal (head sided) or distal (tail sided) pancreatic parenchyma to spinal cord and (b) the contrast ratio (CR) of the lesions to the proximal or distal pancreatic parenchyma, using four manually defined, circular or oval regions of interest (ROIs) (proximal and distal pancreatic parenchyma, lesions, and spinal cord) for each DW image. The ROIs were first placed on DWI_{500}, and then, the size, shape, and location of the ROIs were kept constant for all images of each patient by applying a copy-and-paste function on the

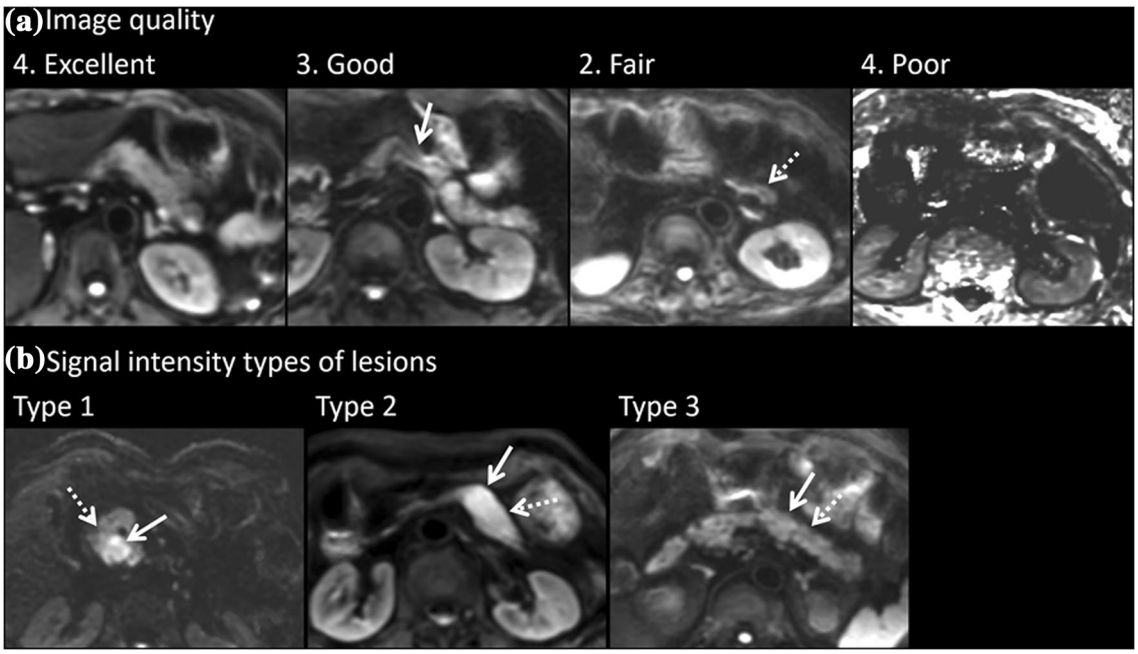

Fig. 2 Example images of image quality grading and signal intensity types of lesions. **a** Image quality was assessed using a 4-point visual score (4, excellent = the whole pancreas is clearly shown without artifacts; 3, good = minor degradation is present but suitable for the evaluation of the whole pancreas; 2, fair = only part of the pancreas is visible; 1, poor = the pancreas is barely visible). **b** Signal intensity types of lesions were classified as follows: type 1, clearly demarcated hyperintensity relative to the surrounding pancreas; type 2, hyperintensity, but with an unclear distal (tail sided) border of the lesions because of hyperintense distal pancreatic parenchyma; and type 3, iso-intensity relative to the surrounding pancreas or no evidence of the lesions (invisible)

monitor. The ROIs were carefully placed to avoid pancreatic ducts, cystic lesions, vessels, peripancreatic fat, or artifacts within the ROIs. If adequate areas were not available for measuring the proximal or distal pancreatic parenchyma due to the locations of the lesions, the sections were excluded from the evaluations. The SIR and CR were calculated using the following formulae [16, 24], using the average SI for the calculations:

$$\text{SIR of the proximal pancreatic parenchyma to the spinal cord } \left(\text{SIR}_{\text{proximal}}\right) = \frac{\text{SI of the proximal pancreatic parenchyma}}{\text{SI of the spinal cord}}$$

$$\text{SIR of the distal pancreatic parenchyma to the spinal cord } \left(\text{SIR}_{\text{distal}}\right) = \frac{\text{SI of the distal pancreatic parenchyma}}{\text{SI of the spinal cord}}$$

$$\text{SIR of the lesion to the spinal cord } \left(\text{SIR}_{\text{lesion}}\right) = \frac{\text{SI of the lesion}}{\text{SI of the spinal cord}}$$

$$\text{CR of the lesion to the proximal pancreatic parenchyma } \left(\text{CR}_{\text{proximal}}\right) = \frac{(\text{SI of the lesion} - \text{SI of the proximal pancreatic parenchyma})}{(\text{SI of the lesion} + \text{SI of the proximal pancreatic parenchyma})}$$

$$\text{CR of the lesion to the distal pancreatic parenchyma } \left(\text{CR}_{\text{distal}}\right) = \frac{(\text{SI of the lesion} - \text{SI of the distal pancreatic parenchyma})}{(\text{SI of the lesion} + \text{SI of the distal pancreatic parenchyma})}.$$

Statistical analyses

Patient demographic data, SIR, and CR were compared between PDAC and AIP by Wilcoxon test and χ^2 test. The size and location of the lesions were determined on MR images. Receiver operating characteristic (ROC) analyses were performed for SIRs and CRs that were significantly different between PDAC and AIP. The image quality was compared among the five DWI protocols by Friedman test, followed by Scheffe's paired comparison. The SI types of lesions were compared among the five DWI protocols by χ^2 test, followed by Wilcoxon signed-rank test. The SIRs and CRs were compared among the five DWI protocols by Friedman test. Cohen's kappa values (κ) or intraclass correlation coefficients (r) were calculated to assess interobserver agreement. Agreement was considered excellent for κ or $r > 0.8$, good for $0.6 < \kappa$ or $r \leq 0.8$, moderate for $0.4 < \kappa$ or $r \leq 0.6$, fair for $0.2 < \kappa$ or $r \leq 0.4$, and poor for κ or $r \leq 0.2$. Coefficient of variation of SIRs and CRs was also calculated and compared between two readers by F test. Data from the first reader were used for the qualitative and quantitative analyses, while those from the second reader were used to calculate interobserver agreement.

All statistical analyses were performed using JMP software (version 14.2.0; SAS Institute Inc., Cary, NC, USA) and BellCurve for Excel (version 3.20; Social Survey Research Information Co., Ltd., Tokyo, Japan). *P*-values < 0.05 were considered statistically significant.

Results

Patients' characteristics

The patients' demographics and clinical characteristics are presented in Table 1. A significant difference was observed in the size of the lesions between PDAC and AIP ($P = 0.001$). Other factors including age, sex, body weight,

Table 1 Patient characteristics

	Pancreatic ductal adenocarcinoma	Autoimmune pancreatitis	*P* value
Number of patients	111	24	
Age (years)	68.9 ± 9.7	64.9 ± 11.9	0.182
Sex (men:women)	69:42	16:8	0.817
Body weight (kg)	55.3 ± 10.3	59.2 ± 10.1	0.059
Lesion location (head:body:tail)	56:21:34	11:8:5	0.266
Lesion size (mm)	22.4 ± 12.4	15.2 ± 7.0	0.001*

Continuous variables were analyzed by Wilcoxon test and are expressed as mean ± standard deviation. Categorical variables were analyzed by the χ^2 test and are expressed as ratios. *$P < 0.05$

Table 2 Results of qualitative and quantitative image analysis on each protocol

	DWI_{500}	DWI_{1000}	$cDWI_{1500}$	$cDWI_{2000}$	$cDWI_{3000}$	*P* value
All patients ($n = 135$)						
Image quality (4:3:2:1)	118:16:1:0	108:26:1:0	90:40:5:0	49:61:23:2	4:42:73:16	< 0.001*
Pancreatic ductal adenocarcinoma ($n = 111$)						
SI types (type 1:2:3)	26:54:31	55:49:7	83:26:2	91:19:1	85:17:9	< 0.001*
$SIR_{proximal}$	0.37 ± 0.12	0.30 ± 0.11	0.22 ± 0.10	0.16 ± 0.09	0.09 ± 0.08	< 0.001*
SIR_{lesion}	0.67 ± 0.21	0.59 ± 0.20	0.48 ± 0.21	0.40 ± 0.22	0.27 ± 0.23	< 0.001*
SIR_{distal}	0.51 ± 0.22	042 ± 0.19	0.30 ± 0.18	0.22 ± 0.17	0.13 ± 0.14	< 0.001*
$CR_{proximal}$	0.29 ± 0.15	0.31 ± 0.15	0.36 ± 0.19	0.39 ± 0.23	0.45 ± 0.31	< 0.001*
CR_{distal}	0.14 ± 0.16	0.19 ± 0.16	0.26 ± 0.21	0.32 ± 0.26	0.41 ± 0.34	< 0.001*
Autoimmune pancreatitis ($n = 24$)						
SI types (type 1:2:3)	13:10:1	21:3:0	22:2:0	22:2:0	18:4:2	0.015*
$SIR_{proximal}$	0.40 ± 0.12	0.34 ± 0.10	0.27 ± 0.08	0.21 ± 0.08	0.13 ± 0.07	< 0.001*
SIR_{lesion}	0.66 ± 0.17	0.63 ± 0.15	0.56 ± 0.17	0.51 ± 0.18	0.41 ± 0.24	< 0.001*
SIR_{distal}	0.47 ± 0.19	0.43 ± 0.19	0.36 ± 0.20	0.31 ± 0.21	0.22 ± 0.21	< 0.001*
$CR_{proximal}$	0.25 ± 0.11	0.31 ± 0.13	0.36 ± 0.15	0.41 ± 0.19	0.48 ± 0.25	< 0.001*
CR_{distal}	0.18 ± 0.13	0.21 ± 0.13	0.24 ± 0.16	0.28 ± 0.32	0.34 ± 0.42	< 0.001*

Image quality was analyzed by Friedman test and is expressed in ratios. SI types of lesions were analyzed by χ^2 test and are expressed in ratios. SIR and CR were analyzed by Friedman test and are expressed as means ± standard deviation. *$P < 0.05$

SI signal intensity, $SIR_{proximal}$ signal intensity ratio of the proximal pancreatic parenchyma to the spinal cord, SIR_{lesion} signal intensity ratio of the proximal pancreas to the lesion, SIR_{distal} signal intensity ratio of the distal pancreatic parenchyma to the spinal cord, $CR_{proximal}$ contrast ratio of the lesion to the proximal pancreatic parenchyma, CR_{distal} contrast ratio of the lesion to the distal pancreatic parenchyma

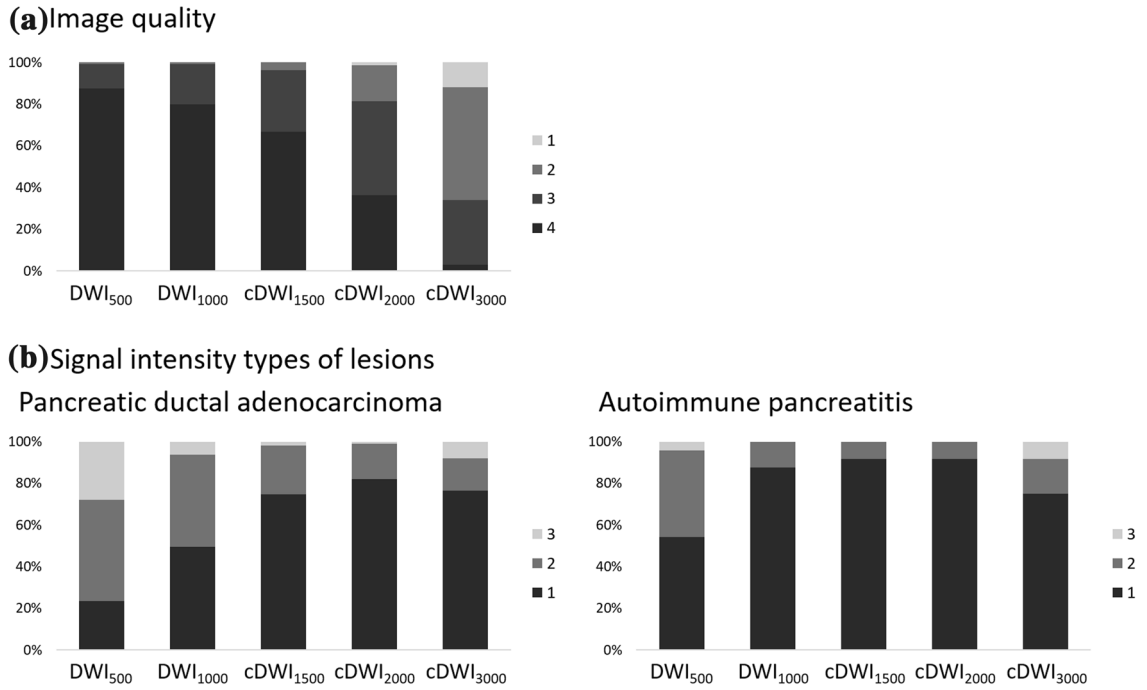

Fig. 3 The breakdown of image quality and signal intensity types of lesions. **a** Image quality. There was a significant difference among the five diffusion-weighted imaging (DWI) protocols ($P < 0.001$). **b** Signal intensity types of lesions. There was a significant difference among the five DWI protocols in both pancreatic ductal adenocarcinoma ($P < 0.001$) and autoimmune pancreatitis ($P = 0.015$). Image quality was analyzed by Friedman test, and signal intensity types of lesions were analyzed by χ^2 test. *cDWI* computed diffusion-weight imaging

and location of the lesions were not significantly different between groups ($P = 0.059$–0.817; Table 1).

Qualitative image analysis

The breakdown of image quality using the five DWI protocols is shown in Table 2 and Fig. 3a. There was a significant difference among the five DWI protocols ($P < 0.001$). In the paired comparison, no significant differences were observed between DWI_{500} and DWI_{1000} ($P = 0.968$), DWI_{500} and $cDWI_{1500}$ ($P = 0.183$), and DWI_{1000} and $cDWI_{1500}$ ($P = 0.548$). In all other combinations, DWI protocols with smaller *b*-values showed significantly higher median image quality than those with higher *b*-values (all $P < 0.001$).

The breakdown of SI types of lesions using the five DWI protocols is shown in Table 2 and Fig. 3b. In PDAC, there were significant differences among the five DWI protocols ($P < 0.001$). In the paired comparison, no significant difference was observed between $cDWI_{1500}$ and $cDWI_{3000}$ ($P = 0.627$). A higher incidence of type 1 lesions was found with $cDWI_{2000}$ than with $cDWI_{3000}$ ($P = 0.002$). In all other combinations, the incidence of type 1 lesions was significantly higher on DWI protocols with higher than with lower *b*-values ($P < 0.001$–0.002). In AIP, there were significant differences among the five DWI protocols ($P = 0.015$). In the paired comparison, the incidence of type 1 lesions was significantly lower with DWI_{500} and $cDWI_{3000}$ than with other protocols ($P = 0.003$ for DWI_{500} vs DWI_{1000}, $P = 0.001$ for DWI_{500} vs $cDWI_{1500}$ and for DWI_{500} vs $cDWI_{2000}$, and $P = 0.022$ for $cDWI_{3000}$ vs $cDWI_{1500}$ and for $cDWI_{3000}$ vs $cDWI_{2000}$). In all other combinations, no significant differences were observed ($P < 0.100$–0.328).

Quantitative image analysis

The mean size of ROIs was as follows: PDAC, 224.1 ± 303.6 mm^2; AIP, 92.9 ± 75.1 mm^2; proximal pancreatic parenchyma, 126.0 ± 49.3 mm^2; distal pancreatic parenchyma, 133.3 ± 70.7 mm^2; spinal cord, 28.3 ± 5.8 mm^2.

The SIR and CR using the five DWI protocols are shown in Table 2 and Fig. 4. There were significant differences in both ratios among the five DWI protocols ($P < 0.001$) for both PDAC and AIP. $SIR_{proximal}$, SIR_{lesion}, and SIR_{distal} decreased, whereas $CR_{proximal}$ and CR_{distal} increased, as the *b*-value increased (Fig. 4). Comparison of PDAC and AIP showed significantly higher $SIR_{proximal}$ and SIR_{lesion} on all cDWIs, and significantly higher SIR_{distal} on $cDWI_{2000}$ and $cDWI_{3000}$ in AIP than in PDAC ($P < 0.001$–0.031; Table 3). In contrast, there were no significant differences for $CR_{proximal}$ and CR_{distal} on all DWI protocols between PDAC and AIP ($P = 0.194$–0.961; Table 3). The area under the ROC curve (AUC) of SIR_{lesion} was significantly lower on $cDWI_{1500}$ than on $cDWI_{2000}$ and $cDWI_{3000}$ ($P < 0.001$), whereas there was no significant difference in the AUC of SIR_{lesion} between $cDWI_{2000}$ and $cDWI_{3000}$ ($P = 0.056$). Moreover, the AUC of SIR_{distal} was significantly higher on $cDWI_{3000}$ than on $cDWI_{2000}$ ($P = 0.001$), while that of $SIR_{proximal}$ was not significantly different among $cDWI_{1500}$, $cDWI_{2000}$, and $cDWI_{3000}$ ($P = 0.514$–1.000; Fig. 5).

Interobserver agreement and coefficient of variation

Interobserver agreement was excellent for the SI types of lesions on DWI_{500}, DWI_{1000}, $cDWI_{1500}$, and $cDWI_{2000}$ ($r = 0.817$–0.848) and for $CR_{proximal}$ on DWI_{500} ($\kappa = 0.814$) and was good for other protocols (r or $\kappa = 0.575$–0.790; Table 4). There was no significant difference in all the

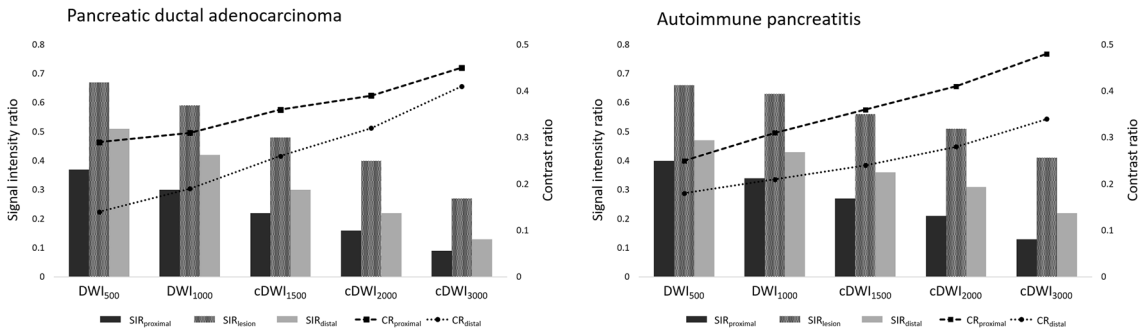

Fig. 4 Differences in signal intensity ratio and contrast ratio among the five diffusion-weighted imaging (DWI) protocols. $SIR_{proximal}$, SIR_{lesion}, and SIR_{distal} decreased, whereas $CR_{proximal}$ and CR_{distal} increased, as the *b*-value increased in both pancreatic ductal adenocarcinoma and autoimmune pancreatitis. *cDWI* computed diffusion-weight imaging, $SIR_{proximal}$ signal intensity ratio of the proximal pancreatic parenchyma to the spinal cord, SIR_{lesion} signal intensity ratio of the proximal pancreas to the lesion, SIR_{distal} signal intensity ratio of the distal pancreatic parenchyma to the spinal cord, $CR_{proximal}$ contrast ratio of the lesion to the proximal pancreatic parenchyma, CR_{distal} contrast ratio of the lesion to the distal pancreatic parenchyma

Table 3 Differences in signal intensity ratio and contrast ratio between pancreatic ductal adenocarcinoma and autoimmune pancreatitis

	Pancreatic ductal adenocarcinoma (n = 111)	Autoimmune pancreatitis (n = 24)	P value
$SIR_{proximal}$			
DWI_{500}	0.37 ± 0.12	0.40 ± 0.12	0.181
DWI_{1000}	0.30 ± 0.11	0.34 ± 0.10	0.176
$cDWI_{1500}$	0.22 ± 0.10	0.27 ± 0.08	0.009*
$cDWI_{2000}$	0.16 ± 0.09	0.21 ± 0.08	0.003*
$cDWI_{3000}$	0.09 ± 0.07	0.13 ± 0.07	0.002*
SIR_{lesion}			
DWI_{500}	0.67 ± 0.21	0.66 ± 0.17	0.895
DWI_{1000}	0.59 ± 0.20	0.63 ± 0.15	0.190
$cDWI_{1500}$	0.48 ± 0.21	0.56 ± 0.17	0.031*
$cDWI_{2000}$	0.40 ± 0.22	0.51 ± 0.18	0.004*
$cDWI_{3000}$	0.27 ± 0.23	0.41 ± 0.24	0.001*
SIR_{distal}			
DWI_{500}	0.51 ± 0.22	0.47 ± 0.19	0.366
DWI_{1000}	0.42 ± 0.19	0.43 ± 0.19	0.649
$cDWI_{1500}$	0.30 ± 0.18	0.36 ± 0.20	0.069
$cDWI_{2000}$	0.22 ± 0.17	0.31 ± 0.21	0.007*
$cDWI_{3000}$	0.13 ± 0.14	0.22 ± 0.21	<0.001*
$CR_{proximal}$			
DWI_{500}	0.29 ± 0.13	0.25 ± 0.11	0.308
DWI_{1000}	0.32 ± 0.15	0.31 ± 0.13	0.961
$cDWI_{1500}$	0.36 ± 0.19	0.36 ± 0.15	0.922
$cDWI_{2000}$	0.39 ± 0.23	0.41 ± 0.19	0.801
$cDWI_{3000}$	0.45 ± 0.31	0.48 ± 0.25	0.760
CR_{distal}			
DWI_{500}	0.14 ± 0.16	0.18 ± 0.13	0.205
DWI_{1000}	0.19 ± 0.16	0.21 ± 0.13	0.428
$cDWI_{1500}$	0.26 ± 0.21	0.24 ± 0.16	0.777
$cDWI_{2000}$	0.32 ± 0.26	0.28 ± 0.20	0.413
$cDWI_{3000}$	0.42 ± 0.34	0.34 ± 0.27	0.194

Data were analyzed by Wilcoxon test and are expressed as mean ± standard deviation. *$P < 0.05$

$SIR_{proximal}$ signal intensity ratio of the proximal pancreatic parenchyma to the spinal cord, SIR_{lesion} signal intensity ratio of the proximal pancreas to the lesion, SIR_{distal} signal intensity ratio of the distal pancreatic parenchyma to the spinal cord, $CR_{proximal}$ contrast ratio of the lesion to the proximal pancreatic parenchyma, CR_{distal} contrast ratio of the lesion to the distal pancreatic parenchyma

coefficient of variation of SIR and CR between two readers (P = 0.106–0.995; Table 5). Case examples are shown in Figs. 6 and 7.

Discussion

This retrospective study revealed that image quality was significantly higher with DWI_{500}, DWI_{1000}, and $cDWI_{1500}$ than with $cDWI_{2000}$ and $cDWI_{3000}$. The incidence of clear hyperintense (type 1) PDAC was the highest on $cDWI_{2000}$, followed by $cDWI_{1500}$ and $cDWI_{3000}$. The incidence of clear hyperintense (type 1) AIP was significantly higher on DWI_{1000}, $cDWI_{1500}$, and $cDWI_{2000}$ than on DWI_{500} and $cDWI_{3000}$. Interobserver agreement was good to excellent for all items. These results suggest that $cDWI_{1500}$ or $cDWI_{2000}$ are the most effective among the five DWI protocols, consistent with a previous report [24].

It is challenging to obtain directly acquired DW images at b-values of 1500 s/mm^2 for the pancreas because the image quality becomes worse and the acquisition time becomes longer as the b-value increases. cDWI can produce DW images without decreasing the signal and in a shorter acquisition time than with directly acquired DWI. Thus, $cDWI_{1500}$ generated from DW images with b-values of 0 and 1000 s/mm^2 may be useful for pancreas imaging. Image contrast on DWI varies greatly with the b-value. At higher b-values, tissues with high water molecule path lengths, such as the pancreatic parenchyma, tend to lose signal rapidly, while tissues with restricted water diffusion, including PDAC, yield relatively higher signals [27, 28]. This explains why the incidence of clear hyperintense (type 1) PDAC on cDW images with b-values ≥1500 s/mm^2 was higher than that on DWI_{500} and DWI_{1000}. Several reports have shown a lower apparent diffusion coefficient value for AIP than for PDAC with b-values 500–1000 s/mm^2 [9, 11, 12, 29], which might explain why the incidence of clear hyperintense (type 1) AIP on DWI_{1000} was equivalent to that on $cDWI_{1500}$ and $cDWI_{2000}$.

In our quantitative image analysis, all SIRs ($SIR_{proximal}$, SIR_{lesion}, and SIR_{distal}) decreased and all CRs ($CR_{proximal}$ and CR_{distal}) increased as the b-value increased. The result of SI decrease can be explained by the fact that higher b-values yield lower signal-to-noise ratio [27, 28]. The result of CR_{distal} is consistent with that of a previous study, while the result of $CR_{proximal}$ is not [24]. The authors reported no significant difference in PDAC to proximal pancreatic parenchymal CR among DWI_{1000}, $cDWI_{1500}$, and $cDWI_{2000}$. This discrepancy may be caused by the different MRI scanners, scanning parameters, and post-processing software used. Further studies are needed to determine the optimal settings of cDWI for PDAC. When comparing PDCA and AIP, $SIR_{proximal}$ and SIR_{lesion} on all cDWI protocols and SIR_{distal} on $cDWI_{2000}$ and $cDWI_{3000}$ were significantly higher in AIP than in PDAC. The results of SIR_{lesion} are consistent to those of previous reports showing lower apparent diffusion coefficient values in AIP than in PDAC when using b-values

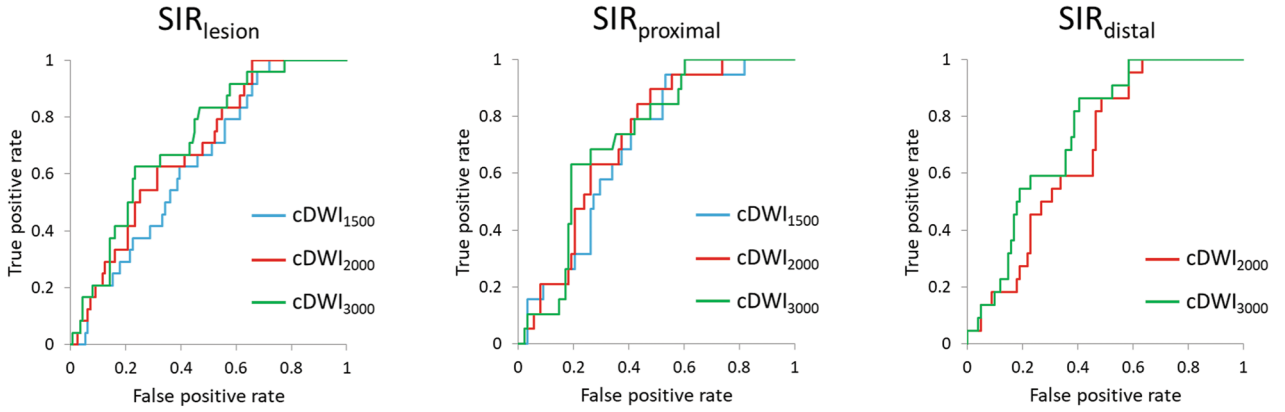

AUC	
$cDWI_{1500}$	0.641 (0.534–0.749)
$cDWI_{2000}$	0.687 (0.583–0.791)
$cDWI_{3000}$	0.720 (0.618–0.821)

Comparison of AUC	*P* value
$cDWI_{1500}$ vs. $cDWI_{2000}$	< 0.001*
$cDWI_{1500}$ vs. $cDWI_{3000}$	< 0.001*
$cDWI_{2000}$ vs. $cDWI_{3000}$	0.056

AUC	
$cDWI_{1500}$	0.691 (0.578–0.805)
$cDWI_{2000}$	0.719 (0.612–0.826)
$cDWI_{3000}$	0.720 (0.624–0.835)

Comparison of AUC	*P* value
$cDWI_{1500}$ vs. $cDWI_{2000}$	0.514
$cDWI_{1500}$ vs. $cDWI_{3000}$	0.982
$cDWI_{2000}$ vs. $cDWI_{3000}$	1.000

AUC	
$cDWI_{2000}$	0.684 (0.581–0.786)
$cDWI_{3000}$	0.743 (0.648–0.838)

Comparison of AUC	*P* value
$cDWI_{2000}$ vs. $cDWI_{3000}$	0.004*

Fig. 5 Receiver operating characteristic analysis of signal intensity ratio. The AUC of SIR_{lesion} was significantly lower on $cDWI_{1500}$ than on $cDWI_{2000}$ and $cDWI_{3000}$ ($P < 0.001$); there was no significant difference between the AUCs of SIR_{lesion} on $cDWI_{2000}$ and $cDWI_{3000}$ ($P = 0.056$). The AUC of SIR_{distal} was significantly higher on $cDWI_{3000}$ than on $cDWI_{2000}$ ($P = 0.001$). The AUC of $SIR_{proximal}$ was not significantly different among $cDWI_{1500}$, $cDWI_{2000}$, and $cDWI_{3000}$ ($P = 0.514$–1.000). The AUCs were compared by χ^2 test. Abbreviations: cDWI, computed diffusion-weight imaging; $SIR_{proximal}$, signal intensity ratio of the proximal pancreatic parenchyma to the spinal cord; SIR_{lesion}, signal intensity ratio of the proximal pancreas to the lesion; SIR_{distal}, signal intensity ratio of the distal pancreatic parenchyma to the spinal cord; AUC, area under the curve

Table 4 Interobserver agreement between two radiologists

	DWI_{500}	DWI_{1000}	$cDWI_{1500}$	$cDWI_{2000}$	$cDWI_{3000}$
Image quality	0.685 (0.535–0.835)	0.702 (0.563–0.842)	0.734 (0.641–0.826)	0.747 (0.648–0.846)	0.670 (0.582–0.758)
SI types of lesions	0.822 (0.737–0.907)	0.848 (0.764–0.933)	0.818 (0.706–0.931)	0.817 (0.690–0.945)	0.740 (0.616–0.864)
$SIR_{proximal}$	0.732 (0.643–0.802)	0.732 (0.643–0.801)	0.689 (0.589–0.768)	0.654 (0.546–0.741)	0.609 (0.490–0.705)
SIR_{lesion}	0.790 (0.696–0.858)	0.751 (0.635–0.835)	0.718 (0.589–0.811)	0.685 (0.538–0.793)	0.647 (0.495–0.761)
SIR_{distal}	0.699 (0.588–0.785)	0.673 (0.554–0.765)	0.653 (0.528–0.749)	0.616 (0.482–0.721)	0.575 (0.432–0.690)
$CR_{proximal}$	0.814 (0.729–0.874)	0.782 (0.670–0.859)	0.774 (0.660–0.854)	0.759 (0.638–0.843)	0.718 (0.581–0.815)
CR_{distal}	0.776 (0.687–0.842)	0.763 (0.670–0.833)	0.742 (0.642–0.817)	0.713 (0.605–0.795)	0.679 (0.561–0.770)

Cohen's kappa values for image quality and signal intensity types of lesions and intraclass correlation coefficients for $SIR_{proximal}$, SIR_{lesion}, SIR_{distal}, $CR_{proximal}$, and CR_{distal} are presented with the 95% confidence interval in parentheses

SI signal intensity, $SIR_{proximal}$ signal intensity ratio of the proximal pancreatic parenchyma to the spinal cord, SIR_{lesion} signal intensity ratio of the proximal pancreas to the lesion, SIR_{distal} signal intensity ratio of the distal pancreatic parenchyma to the spinal cord, $CR_{proximal}$ contrast ratio of the lesion to the proximal pancreatic parenchyma, CR_{distal} contrast ratio of the lesion to the distal pancreatic parenchyma

500–1000 s/mm^2 [9, 11, 12, 29]. Increased cellularity due to dense infiltration of plasma cells and lymphocytes, chronic inflammatory changes with fibrosis, and edematous changes in AIP may be associated to the high signal intensity [5, 30]. It is not clear why $SIR_{proximal}$ and SIR_{distal} AIP were higher in AIP than in PDAC; however, the surrounding pancreatic

Table 5 Coefficient of variation between two radiologists

	DWI_{500}			DWI_{1000}			$cDWI_{1500}$			$cDWI_{2000}$			$cDWI_{3000}$		
	R1	R2	*P*	R1	R2	*P*	R1	R2	*P*	R1	R2	*P*	R1	R2	*P*
$SIR_{proximal}$	0.290	0.270	0.955	0.328	0.297	0.528	0.404	0.370	0.209	0.534	0.431	0.465	0.818	0.543	0.374
SIR_{lesion}	0.302	0.260	0.413	0.329	0.300	0.803	0.411	0.402	0.288	0.515	0.472	0.461	0.710	0.610	0.646
SIR_{distal}	0.435	0.383	0.828	0.466	0.383	0.254	0.615	0.548	0.969	0.797	0.685	0.656	1.192	0.913	0.939
$CR_{proximal}$	0.449	0.417	0.466	0.490	0.632	0.106	0.523	0.797	0.116	0.589	0.899	0.254	0.674	1.092	0.136
CR_{distal}	0.996	0.755	0.492	0.776	0.674	0.836	0.759	0.648	0.800	0.783	0.731	0.830	0.814	0.715	0.995

Data were analyzed by *F* test

R1 reader 1, *R2* reader 2, *P P* value, $SIR_{proximal}$ signal intensity ratio of the proximal pancreatic parenchyma to the spinal cord, SIR_{lesion} signal intensity ratio of the proximal pancreas to the lesion, SIR_{distal} signal intensity ratio of the distal pancreatic parenchyma to the spinal cord, $CR_{proximal}$ contrast ratio of the lesion to the proximal pancreatic parenchyma, CR_{distal} contrast ratio of the lesion to the distal pancreatic parenchyma

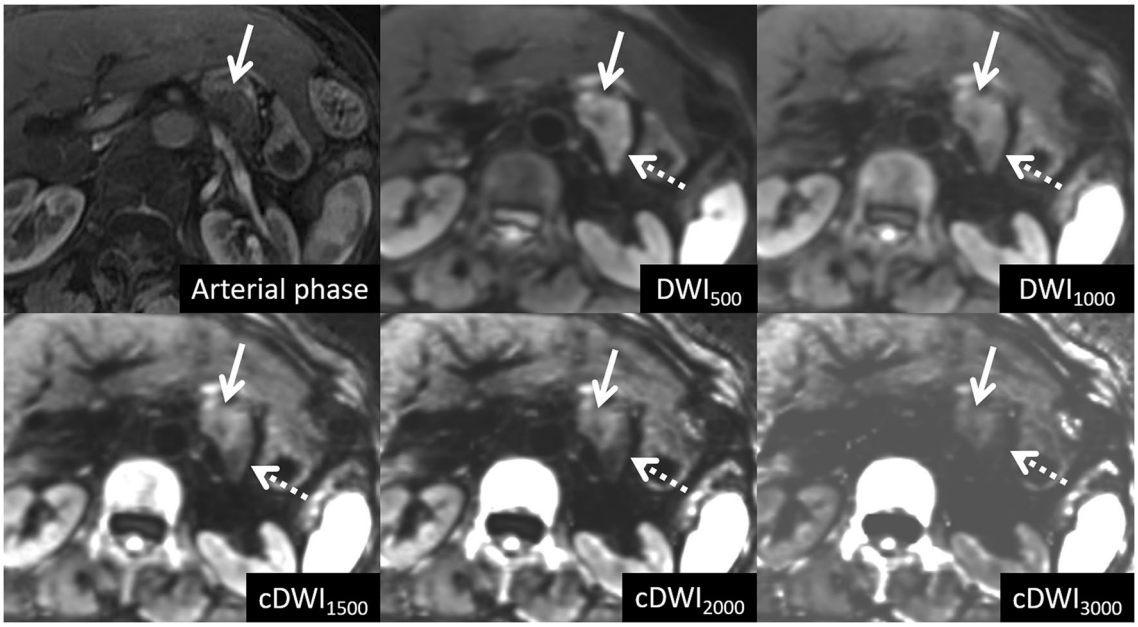

Fig. 6 Representative images of pancreatic ductal adenocarcinoma in a 78-year-old woman. Arterial phase of gadoxetate disodium-enhanced 3D fat-saturated T1-weighted imaging (repetition time/echo time, 3.44/1.43; flip angle, 12°) shows a hypointense lesion measuring 22 mm in diameter (arrow) in the pancreatic tail. On diffusion-weighted imaging (DWI) with a *b*-value of 500 s/mm^2 (DWI_{500}), the lesion (arrow) shows hyperintensity with an unclear distal border (type 2). On DWI with a *b*-value of 1000 s/mm^2 (DWI_{1000}) and computed DWI with target *b*-value of 1500 ($cDWI_{1500}$), 2000 ($cDWI_{2000}$), and 3000 ($cDWI_{3000}$) s/mm^2, the lesion (arrow) shows clear hyperintensity relative to the distal pancreatic parenchyma (dotted arrow) (type 1); however, on $cDWI_{3000}$, the distal pancreatic parenchyma is almost invisible

parenchyma may also be infiltrated with plasma cells and lymphocytes, although this cannot be detected by imaging because of its autoimmune nature [31]. In this study, we found no significant differences in $CR_{proximal}$ and CR_{distal} on all DWI protocols between PDAC and AIP. Therefore, it may be difficult to distinguish AIP from PDAC by visual evaluation. The AUC of SIR_{lesion} on $cDWI_{1500}$ was significantly lower than that on $cDWI_{2000}$ and $cDWI_{3000}$, whereas there was no significant difference between the AUCs of SIR_{lesion} on $cDWI_{2000}$ and $cDWI_{3000}$. The AUC of SIR_{distal} on $cDWI_{3000}$ was significantly higher than that on $cDWI_{2000}$ ($P = 0.001$). These results indicate that $cDWI_{2000}$ and $cDWI_{3000}$ are better for quantitative analysis than $cDWI_{1500}$; however, lower image quality may be a problem in clinical practice. Validation studies are desired as a next step.

Our study has some limitations. First, AIP of various inflammatory activities was included in this study. The phase of inflammation can influence signal intensity on DWI because of differences in dense infiltration of plasma cells and lymphocytes or edematous changes. Second, significant

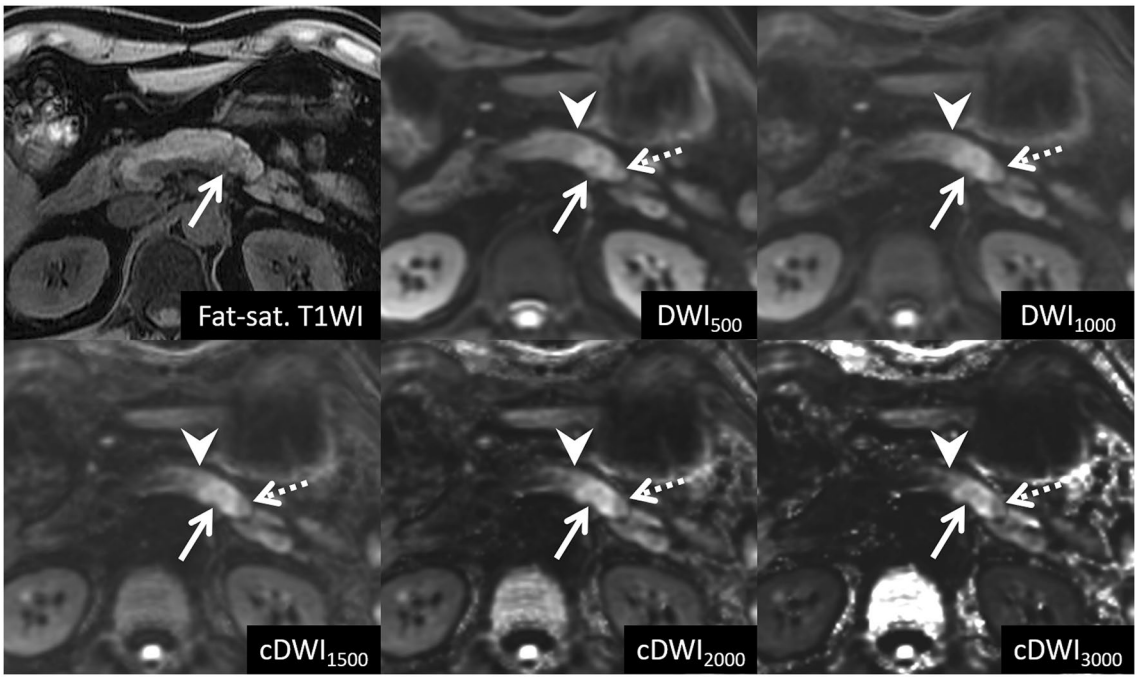

Fig. 7 Representative images of autoimmune pancreatitis in a 48-year-old man. Unenhanced 3D fat-saturated T1-weighted imaging (repetition time/echo time, 4.34/1.43; flip angle, 15°) shows a vague hypointense lesion measuring 18 mm in diameter (arrow) in the pancreatic tail. On diffusion-weighted imaging (DWI) with a *b*-value of 500 (DWI_{500}) and 1000 (DWI_{1000}) s/mm^2, and computed DWI with target *b*-value of 1500 ($cDWI_{1500}$), 2000 ($cDWI_{2000}$), and 3000 ($cDWI_{3000}$) s/mm^2, the lesion (arrow) shows hyperintensity relative to the proximal (arrowhead) and distal pancreatic parenchyma (dotted arrow) (type 1); however, on DWI_{500}, the border between the lesion and the pancreatic parenchyma is somewhat unclear

differences in the size of lesions were observed between PDAC and AIP, possibly due to the retrospective study design. Degeneration or necrotic changes are observed more frequently in larger lesions, especially in PDAC, which can also influence the signal intensity of DWI. Third, the retrospective nature and relatively small number of AIP cases in this study were also limitations. Further prospective studies with a larger sample size are necessary.

In summary, $cDWI_{1500}$ or $cDWI_{2000}$ generated from DW images obtained with *b*-values of 0 and 1000 s/mm^2 were found to be the most effective among the five tested DWI protocols (DWI_{500}, DWI_{1000}, $cDWI_{1500}$, $cDWI_{2000}$, and $cDWI_{3000}$) for visualizing PDAC and focal AIP; however, the AUC of SIR_{lesion} was significantly lower on $cDWI_{1500}$ than on $cDWI_{2000}$ and $cDWI_{3000}$. Therefore, the combination of $cDWI_{1500}$ and $cDWI_{2000}$/$cDWI_{3000}$ may be effective in diagnosing AIP.

Funding This research received no specific grant.

Compliance with ethical standards

Conflict of interest The authors declare that they have no conflict of interest.

References

1. Bray F, Ferlay J, Soerjomataram I, Siegel RL, Torre LA, Jemal A (2018) Global cancer statistics 2018: GLOBOCAN estimates of incidence and mortality worldwide for 36 cancers in 185 countries. CA Cancer J Clin 68:394–424. https://doi.org/10.3322/caac.21492
2. Yabar CS, Winter JM (2016) Pancreatic cancer: a review. Gastroenterol Clin North Am 45:429–445. https://doi.org/10.1016/j.gtc.2016.04.003.
3. McGuigan A, Kelly P, Turkington RC, Jones C, Coleman HG, McCain RS (2018) Pancreatic cancer: A review of clinical diagnosis, epidemiology, treatment and outcomes. World J Gastroenterol 24:4846–4861. https://doi.org/10.3748/wjg.v24.i43.4846.
4. Rawla P, Sunkara T, Gaduputi V (2019) Epidemiology of pancreatic cancer: global trends, etiology and risk factors. World J Oncol 10:10–27. https://doi.org/10.14740/wjon1166.
5. Nagpal SJS, Sharma A, Chari ST (2018) Autoimmune pancreatitis. Am J Gastroenterol 113:1301. https://doi.org/10.1038/s41395-018-0146-0.
6. Kwon JH, Kim JH, Kim SY, et al (2019) Differentiating focal autoimmune pancreatitis and pancreatic ductal adenocarcinoma: contrast-enhanced MRI with special emphasis on the arterial phase. Eur Radiol 29:5763–5771. https://doi.org/10.1007/s00330-019-06200-0.
7. Lee S, Kim JH, Kim SY, et al (2018) Comparison of diagnostic performance between CT and MRI in differentiating non-diffuse-type autoimmune pancreatitis from pancreatic ductal adenocarcinoma. Eur Radiol 28:5267–5274. https://doi.org/10.1007/s00330-018-5565-1.

8. Kim HJ, Kim YK, Jeong WK, Lee WJ, Choi D (2015) Pancreatic duct "Icicle sign" on MRI for distinguishing autoimmune pancreatitis from pancreatic ductal adenocarcinoma in the proximal pancreas. Eur Radiol 25:1551–1560. https://doi.org/10.1007/s00330-014-3548-4.
9. Hur BY, Lee JM, Lee JE, et al (2012) Magnetic resonance imaging findings of the mass-forming type of autoimmune pancreatitis: comparison with pancreatic adenocarcinoma. J Magn Reson Imaging 36:188–197. https://doi.org/10.1002/jmri.23609.
10. Oki H, Hayashida Y, Oki H, et al (2015) DWI findings of autoimmune pancreatitis: comparison between symptomatic and asymptomatic patients. J Magn Reson Imaging 41:125–131. https://doi.org/10.1002/jmri.24508.
11. Choi SY, Kim SH, Kang TW, Song KD, Park HJ, Choi YH (2016) Differentiating mass-forming autoimmune pancreatitis from pancreatic ductal adenocarcinoma on the basis of contrast-enhanced MRI and DWI findings. AJR Am J Roentgenol 206:291–300. https://doi.org/10.2214/AJR.15.14974.
12. Muhi A, Ichikawa T, Motosugi U, et al (2012) Mass-forming autoimmune pancreatitis and pancreatic carcinoma: differential diagnosis on the basis of computed tomography and magnetic resonance cholangiopancreatography, and diffusion-weighted imaging findings. J Magn Reson Imaging 35:827–836. https://doi.org/10.1002/jmri.22881.
13. Kovac JD, Duric-Stefanovic A, Dugalic V, et al (2019) CT perfusion and diffusion-weighted MR imaging of pancreatic adenocarcinoma: can we predict tumor grade using functional parameters? Acta Radiol 60:1065–1073. https://doi.org/10.1177/0284185118812202.
14. Zong RL, Geng L, Wang X, Xie D (2019) Diagnostic performance of apparent diffusion coefficient for prediction of grading of pancreatic neuroendocrine tumors: a systematic review and meta-analysis. Pancreas 48:151–160. https://doi.org/10.1097/MPA.0000000000001212.
15. Kawakami S, Fukasawa M, Shimizu T, et al (2019) Diffusion-weighted image improves detectability of magnetic resonance cholangiopancreatography for pancreatic ductal adenocarcinoma concomitant with intraductal papillary mucinous neoplasm. Medicine (Baltimore) 98:e18039. https://doi.org/10.1097/MD.0000000000018039.
16. Fukukura Y, Shindo T, Hakamada H, et al (2016) Diffusion-weighted MR imaging of the pancreas: optimizing b-value for visualization of pancreatic adenocarcinoma. Eur Radiol 26:3419–3427. https://doi.org/10.1007/s00330-015-4174-5.
17. Higaki T, Nakamura Y, Tatsugami F, et al (2018) Introduction to the technical aspects of computed diffusion-weighted imaging for radiologists. Radiographics 38:1131–1144. https://doi.org/10.1148/rg.2018170115.
18. Ueno YR, Tamada T, Takahashi S, et al (2018) Computed diffusion-weighted imaging in prostate cancer: basics, advantages, cautions, and future prospects. Korean J Radiol 19:832–837. https://doi.org/10.3348/kjr.2018.19.5.832.
19. Tamura T, Takasu M, Higaki T, et al (2019) How to improve the conspicuity of breast tumors on computed high b-value diffusion-weighted imaging. Magn Reson Med Sci 18:119–125. https://doi.org/10.2463/mrms.mp.2018-0011.
20. Akagi M, Nakamura Y, Higaki T, et al (2018) Preliminary results of high-precision computed diffusion weighted imaging for the diagnosis of hepatocellular carcinoma at 3 Tesla. J Comput Assist Tomogr 42:373–379. https://doi.org/10.1097/RCT.0000000000000702.
21. Moribata Y, Kido A, Fujimoto K, et al (2017) Feasibility of computed diffusion weighted imaging and optimization of b-value in cervical cancer. Magn Reson Med Sci 16:66–72. https://doi.org/10.2463/mrms.mp.2015-0161.
22. Takeuchi M, Matsuzaki K, Harada M (2016) Computed diffusion-weighted imaging for differentiating decidualized endometrioma from ovarian cancer. Eur J Radiol 85:1016–1019. https://doi.org/10.1016/j.ejrad.2016.03.009.
23. Yamashita K, Hiwatashi A, Togao O, et al (2019) Improved visualization of middle ear cholesteatoma with computed diffusion-weighted imaging. Magn Reson Med Sci 18:233–237. https://doi.org/10.2463/mrms.tn.2018-0068.
24. Fukukura Y, Kumagae Y, Hakamada H, et al (2017) Computed diffusion-weighted MR imaging for visualization of pancreatic adenocarcinoma: Comparison with acquired diffusion-weighted imaging. Eur J Radiol 95:39–45. https://doi.org/10.1016/j.ejrad.2017.07.022.
25. Tokunaga K, Arizono S, Shimizu H, et al (2020) Optimizing b-values for accurate depiction of pancreatic cancer with tumor-associated pancreatitis on computed diffusion-weighted imaging. Clin Imaging 61:20–26. https://doi.org/10.1016/j.clinimag.2020.01.007.
26. Shimosegawa T, Working Group Members of the Japan Pancreas S, Research Committee for Intractable Pancreatic Disease by the Ministry of Labor H, Welfare of J (2012) The amendment of the Clinical Diagnostic Criteria in Japan (JPS2011) in response to the proposal of the International Consensus of Diagnostic Criteria (ICDC) for autoimmune pancreatitis. Pancreas 41:1341–1342. https://doi.org/10.1097/MPA.0b013e3182706ed5.
27. Moore WA, Khatri G, Madhuranthakam AJ, Sims RD, Pedrosa I (2014) Added value of diffusion-weighted acquisitions in MRI of the abdomen and pelvis. AJR Am J Roentgenol 202:995–1006. https://doi.org/10.2214/AJR.12.9563.
28. Koh DM, Lee JM, Bittencourt LK, Blackledge M, Collins DJ (2016) Body diffusion-weighted MR imaging in oncology: imaging at 3 T. Magn Reson Imaging Clin N Am 24:31–44. https://doi.org/10.1016/j.mric.2015.08.007.
29. Kamisawa T, Takuma K, Anjiki H, et al (2010) Differentiation of autoimmune pancreatitis from pancreatic cancer by diffusion-weighted MRI. Am J Gastroenterol 105:1870–1875. https://doi.org/10.1097/MD.0000000000018039.
30. Majumder S, Takahashi N, Chari ST (2017) Autoimmune pancreatitis. Dig Dis Sci 62:1762–1769. https://doi.org/10.1007/s10620-017-4541-y.
31. Hart PA, Zen Y, Chari ST (2015) Recent Advances in autoimmune pancreatitis. Gastroenterology 149:39–51. https://doi.org/10.1053/j.gastro.2015.03.010.